Land Surface Temperature Retrieval Methods From Landsat-8 Thermal Infrared Sensor Data

Juan C. Jiménez-Muñoz, José A. Sobrino, Dražen Skoković, Cristian Mattar, and Jordi Cristóbal

***Abstract*—The importance of land surface temperature (LST) retrieved from high to medium spatial resolution remote sensing data for many environmental studies, particularly the applications related to water resources management over agricultural sites, was a key factor for the final decision of including a thermal infrared (TIR) instrument on board the Landsat Data Continuity Mission or Landsat-8. This new TIR sensor (TIRS) includes two TIR bands in the atmospheric window between 10 and 12 μm, thus allowing the application of split-window (SW) algorithms in addition to single-channel (SC) algorithms or direct inversions of the radiative transfer equation used in previous sensors on board the Landsat platforms, with only one TIR band. In this letter, we propose SC and SW algorithms to be applied to Landsat-8 TIRS data for LST retrieval. Algorithms were tested with simulated data obtained from forward simulations using atmospheric profile databases and emissivity spectra extracted from spectral libraries. Results show mean errors typically below 1.5 K for both SC and SW algorithms, with slightly better results for the SW algorithm than for the SC algorithm with increasing atmospheric water vapor contents.**

***Index Terms*—Land surface temperature (LST), Landsat-8, Landsat Data Continuity Mission (LDCM), single-channel (SC) algorithm, split-window (SW) algorithm, thermal infrared (TIR).**

I. Introduction

THE recent launch of the Landsat-8 satellite (also known as Landsat Data Continuity Mission, LDCM) in February 2013 ensures the continuity of remote sensing data at high spatial resolution acquired by instruments on board previous Landsat satellites such as the Multispectral Scanner System, the Thematic Mapper (TM), and the Enhanced Thematic Mapper Plus (ETM+). Landsat-8 carries two sensors, i.e., the Operational Land Imager (OLI) and the thermal infrared sensor (TIRS). OLI collects data at a 30-m spatial resolution with eight bands located in the visible and near-infrared and in the shortwave infrared regions of the electromagnetic spectrum, plus an additional panchromatic band at 15-m spatial resolution. TIRS measures the TIR radiance at 100-m spatial resolution using two bands located in the atmospheric window between 10 and 12 μm [1].

Although an OLI-like sensor was included since the beginning of the LDCM design, thermal imaging was initially excluded from the LDCM requirements. The increase in applications using Landsat5 TM or Landsat7 ETM+ thermal data in recent years, particularly of applications related to water resource management over agricultural sites, was a key factor to finally include a TIR sensor as a part of LDCM [1]. These applications rely on the solution for heat fluxes involved in the energy balance equation, and ultimately on the evapotranspiration retrieval, which can be only addressed in a proper way if TIR data are available. In particular, land surface temperature (LST) is a key variable to be retrieved from TIR data, which also plays an important role in other geo–biophysical studies [2]–[4].

In this letter, we propose some methods for LST retrieval from the new Landsat-8 TIR instrument. Recently, the U.S. Geological Survey has reported a calibration problem of TIRS bands caused by stray light. The Landsat-8 team is currently solving the problem, and a reprocessing of Landsat-8 imagery is planned (http://landsat.usgs.gov/mission_headlines2014.php). Therefore, in this letter, we test the algorithms with an extensive simulated data set constructed from forward simulations for a number of input data. The LST retrieval methods presented in this letter were selected because of their practical applicability to Landsat-8 data. This letter does not attempt to review different LST/emissivity retrieval methodologies, as detailed, for example, in two recent publications [5], [6].

II. LST Algorithms

A. Landsat-8 TIRS Bands

The main difference between the new TIRS and previous TM/ETM sensors (apart from differences related to sensor design) is the presence of two TIR bands in the atmospheric window between 10 and 12 μm, which represents an advancement over the single thermal band present on TM and ETM sensors (see Fig. 1). Since the previous single band has been split into two TIR bands, the bandwidths of TIRS bands are narrower than the previous TM/ETM TIR band. The presence of two TIR bands opens the possibility to apply split-window (SW) algorithms instead of single-channel (SC) algorithms for LST retrieval, as will be presented in subsequent sections.

The noise-equivalent delta temperature (NEΔT) for the TIR bands is estimated at 0.4 K (prelaunch values), which is similar to the NEΔT of the previous TM sensors (0.5 K) [7]. Later calibration activities estimated the NEΔT of TM/ETM sensors at around 0.2–0.3 K [8]. Further sensor technical details are presented in [1].

Manuscript received February 21, 2014; revised March 11, 2014; accepted March 12, 2014. This work was supported in part by the European Union, CEOP-AEGIS, through project FP7-ENV-2007-1, under Grant 212921; the Ministerio de Economía y Competitividad, Earth Observation: Optical Data Calibration and Information Extraction, through project AYA2008-0595-C04-01; CEOS-Spain, through project AYA2011-29334-C02-01; the Universitat de València, UV-INV-PRECOMP13-115366; and the University of Chile, Program U-INICIA VID 2012, under Grant U-INICIA 4/0612.

J. C. Jiménez-Muñoz, J. A. Sobrino, and D. Skoković are with the Global Change Unit, Image Processing Laboratory, University of Valencia, 46071 Valencia, Spain (e-mail: jcjm@uv.es; sobrino@uv.es; drazen.skokovic@uv.es).

C. Mattar is with the Laboratory for Analysis of the Biosphere, Department of Environmental Sciences and Renewable Natural Resources, University of Santiago, Santiago 11315, Chile (e-mail: cmattar.lab@gmail.com).

J. Cristóbal is with the Geophysical Institute, University of Alaska Fairbanks, Fairbanks, AK 99775-7320 USA (e-mail: jordi.cristobal@gi.alaska.edu).

Digital Object Identifier 10.1109/LGRS.2014.2312032

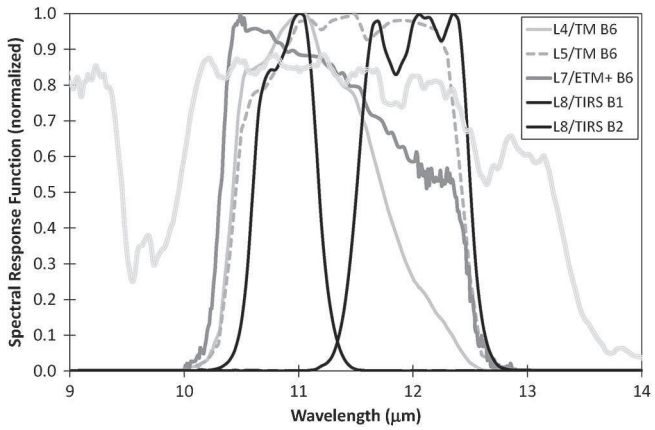

Fig. 1. Spectral response functions for the thermal bands of the different sensors on board the Landsat platforms. Effective wavelength (in micrometers) for each band is 11.154 (L4/TM), 11.457 (L5/TM), 11.269 (L7/ETM+), 10.904 (L8/TIRS B1), and 12.003 (L8/TIRS B2). The atmospheric transmissivity for a standard atmosphere is also plotted in light gray.

B. SC Algorithm

The SC algorithm developed by Jiménez-Muñoz *et al.* [9] retrieves LST (T_s) using the following general equation:

$$T_s = \gamma \left[\frac{1}{\varepsilon}(\psi_1 L_{sen} + \psi_2) + \psi_3 \right] + \delta \tag{1}$$

where ε is the surface emissivity, and (γ, δ) are two parameters given by

$$\gamma \approx \frac{T_{\text{sen}}^2}{b_\gamma L_{\text{sen}}}; \quad \delta \approx T_{\text{sen}} - \frac{T_{\text{sen}}^2}{b_\gamma} \tag{2}$$

where T_{sen} is the at-sensor brightness temperature; $b_\gamma = c_2/\lambda$ (1324 for TIRS-1 and 1199 K for TIRS-2); and ψ_1, ψ_2, and ψ_3 are the so-called atmospheric functions, given by

$$\psi_1 = \frac{1}{\tau}; \quad \psi_2 = -L_d - \frac{L_u}{\tau}; \quad \psi_3 = L_d. \tag{3}$$

The practical approach proposed in the SC algorithm consists of the approximation of the atmospheric functions defined in (3) versus the atmospheric water vapor content W from a second-order polynomial fit, expressed in matrix notation as follows ($\Psi = \text{CW}$):

$$\begin{bmatrix} \psi_1 \\ \psi_2 \\ \psi_3 \end{bmatrix} = \begin{bmatrix} c_{11} & c_{12} & c_{13} \\ c_{21} & c_{22} & c_{23} \\ c_{31} & c_{32} & c_{33} \end{bmatrix} \begin{bmatrix} w^2 \\ w \\ 1 \end{bmatrix} \tag{4}$$

where coefficients c_{ij} are obtained by simulation. Alternatively, if atmospheric parameters τ, L_u, and L_d are known, the atmospheric functions can be calculated from (3), thus avoiding the empirical relationship versus w. Note also that the SC algorithm can be applied to any of the two TIRS bands. However, since TIRS-1 is located in a lower atmospheric absorption region (high atmospheric transmissivity values, see Fig. 1), it is preferable to use this band.

C. SW Algorithm

The SW technique uses two TIR bands typically located in the atmospheric window between 10 and 12 μm. The basis of the technique is that the radiance attenuation for atmospheric absorption is proportional to the radiance difference of simultaneous measurements at two different wavelengths, each of them being subject to different amounts of atmospheric absorption [10]. The SW algorithm proposed in this letter is based on the mathematical structure proposed by Sobrino *et al.* [11] and applied to different Earth Observation sensors in [12], i.e.,

$$T_s = T_i + c_1(T_i - T_j) + c_2(T_i - T_j)^2 + c_0 + (c_3 + c_4 w)(1 - \varepsilon) + (c_5 + c_6 w)\Delta\varepsilon \tag{5}$$

where T_i and T_j are the at-sensor brightness temperatures at the SW bands i and j (in kelvins), ε is the mean emissivity, $\varepsilon = 0.5\,(\varepsilon_i + \varepsilon_j)$, $\Delta\varepsilon$ is the emissivity difference, $\Delta\varepsilon = (\varepsilon_i - \varepsilon_j)$, w is the total atmospheric water vapor content (in $\text{g} \cdot \text{cm}^{-2}$), and c_0 to c_6 are the SW coefficients to be determined from simulated data.

III. Simulated Data for Algorithm Coefficient Retrieval and Testing

Both the SC and the SW algorithms require the retrieval of several coefficients; in the case of the SC, the coefficients occur in the relationship between the atmospheric functions and the water vapor [see (4)], and in the case of the SW algorithm, the coefficients appear in the SW algorithm itself [see (5)]. These coefficients are retrieved from statistical fits performed over a simulated database. Simulated data are obtained from atmospheric profile data sets used as inputs to the MODTRAN radiative transfer code [13]. MODTRAN spectral outputs are convoluted with the spectral response functions to finally obtain the band-averaged values of the atmospheric parameters τ, L_u, and L_d. In the case of the SW algorithms, where the at-sensor brightness temperatures need to be simulated, different emissivity spectra (108 samples) extracted from the advanced spaceborne thermal emission and reflection radiometer library are also used [14]. Additional details on the simulation procedure for the SW and SC algorithms can be found in [9] and [12].

In previous work [9], [15] different atmospheric profile databases [Thermodynamic Initial Guess Retrieval (TIGR) and STanDard atmospheres in included in MODTRAN code (STD)] were used to derive the atmospheric functions (TIGR_{61}, TIGR_{1761}, TIGR_{2311}, and STD_{66}, where the subindex refers to the number of atmospheric profiles included in each database). However, in this letter, a recently created atmospheric profile database, i.e., Global Atmospheric Profiles from Reanalysis Information (GAPRI), has been used to derive the coefficients of the algorithms, whereas the TIGR and STD databases were used only for validation purposes (algorithms testing using an independent database). The GAPRI database is a comprehensive compilation of selected atmospheric profiles (geopotential height, atmospheric pressure, air temperature, and relative humidity) at a global scale derived from ERA-Interim reanalysis data during 2011 [16]. Atmospheric profiles were extracted at 29 vertical levels from a global spatial grid of about $0.75^\circ \times 0.75^\circ$ latitude–longitude. The GAPRI database used

in this study contains 4714 atmospheric profiles selected over land (GAPRI_{4714}), covering tropical, midlatitude, subarctic, and arctic weather conditions. A detailed description of the GAPRI database is provided in Mattar *et al.* [17].

To account for differences between LST and air temperature (temperature at the first layer in the atmospheric profile), the following variations were considered for the LST: $T_0 - 5$, T_0, $T_0 + 5$, $T_0 + 10$, and $T_0 + 20$, where T_0 is the temperature at the first layer. These temperature steps were used in other studies [12], although the highest temperature step $(T_0 + 20)$ could be too low for desert regions. Therefore, the number of atmospheric profiles included in each database must be multiplied by 5 when these variations are considered; in the case of the SW algorithm, where 108 surface emissivities are also used in the simulation, this number must be additionally multiplied to obtain the total amount of simulated cases.

IV. Results

A. SC Coefficients and Sensitivity Analysis

The following coefficients were obtained for the atmospheric functions [see (3) and (4)] of the SC algorithm (TIRS-1 band, 10.9 μm) using the GAPRI_{4838} database:

$$C = \begin{bmatrix} 0.04019 & 0.02916 & 1.01523 \\ -0.38333 & -1.50294 & 0.20324 \\ 0.00918 & 1.36072 & -0.27514 \end{bmatrix} \quad (6)$$

with a Pearson's linear correlation coefficient higher than 0.98 for the three atmospheric functions. Since total column water vapor w is the main input to the algorithm (except for surface emissivity), we tested the sensitivity of the algorithm to variations in w of ± 0.5 g $\cdot$ cm^{-2} for all the simulated data obtained from the GAPRI database. Bias (LST for a given variation of w minus LST when nominal w_0 value is considered) values were (0.2 ± 0.7) K for $w_0 - 0.5$, and (-0.5 ± 1.0) K for $w_0 + 0.5$, with respective root mean square errors (RMSEs) of 0.8 and 1.1 K.

B. SW Coefficients and Sensitivity Analysis

Coefficients for the SW algorithm [see (5)] are presented in Table I. The standard error of estimation in the statistical fit (δ_{alg}) was 0.6 K, with a Pearson's linear correlation coefficient of 0.98. The sensitivity analysis was performed using the procedure explained in [12], where the different contributions to the final error on the LST are calculated from the different derivatives according to the classical error theory. The different input values to particular uncertainties were 0.4 K for the sensor's NEΔT, 0.01 for the surface emissivity, and 0.5 g $\cdot$ cm^{-2} for the atmospheric water vapor content. Results are also included in Table I, and the final error for the LST was 2.1 K. Major contributions to this error are due to the NEΔT (1.5 K) and the uncertainty of the surface emissivity (1.4 K). Furthermore, Table I includes the LST error when the sensor's NEΔT is assumed to be only 0.1 K (this is not true for Landsat-8 TIRS bands, but this value is more representative of typical low-resolution polar orbiting sensors). In this case, the contribution of the NEΔT to the total LST error is significantly reduced (from 1.5 to 0.4 K), and total LST error is then 1.5 K.

TABLE I
Coefficients for the SW Algorithm Given by (5) Obtained From Simulated Data Using the MAPRI_{4714} Database. Results Obtained in the Sensitivity Analysis Are Also Provided: δ_{alg}, Standard Error of Estimation in the Linear Regression; $\delta_{\mathrm{NE}\Delta\mathrm{T}}$, Error Due to the Noise Equivalent Delta Temperature; $\delta\varepsilon$, Error Due to the Uncertainty of the Surface Emissivity; δ_w, Error Due to the Uncertainty on the Atmospheric Water Vapor Content; e(LST), Total Error in the LST. Pearson's Correlation Coefficient (r) Is Also Included

Coefficients		Sensitivity Analysis	
c_0	-0.268		
c_1	1.378	δ_{alg}	0.6
c_2	0.183	$\delta_{\mathrm{NE}\Delta\mathrm{T}}$	1.5 (0.4*)
c_3	54.30	δ_{ε}	1.4
c_4	-2.238	δ_{w}	0.09
c_5	-129.20		
c_6	16.40	***e(LST)***	***2.1 (1.5*)***
r	*0.984*		

*Values for NEΔT=0.1K

TABLE II
Test of the SC and SW Algorithms Using Independent Simulated Data. ΔW Is the Atmospheric Water Vapor Range (in g $\cdot$ cm^{-2}), N Is the Number of Simulated Data, Bias Is the Difference Between Retrieved and Reference LST, σ Is the 1-Sigma Standard Deviation, RMSE Is the Root Mean Square Error, and r Is the Pearson's Correlation Coefficient

Data	Alg.	ΔW	N	Bias (K)	σ (K)	RMSE (K)	r
TIGR_{61}	SW	0-6	32940	-0.1	1.2	1.2	0.997
	SC	0-6	32940	-2.7	3.0	4.0	0.982
	SC	0-3	17820	-1.2	1.5	1.9	0.996
	SC	3-6	15120	-4.5	3.2	5.6	0.954
TIGR_{1761}	SW	0-6	950940	0.0	0.6	0.6	0.999
	SC	0-6	950940	-1.1	1.7	2.0	0.996
	SC	0-3	886680	-0.8	0.9	1.2	0.999
	SC	3-6	58860	-4.0	3.5	5.4	0.957
TIGR_{2311}	SW	0-6	249588	0.4	1.0	1.1	0.999
	SC	0-6	249588	-2.2	3.7	4.3	0.981
	SC	0-3	186732	-1.0	1.1	1.5	0.998
	SC	3-6	54216	-4.5	4.6	6.5	0.936
STD_{66}	SW	0-6	35640	-0.2	0.9	0.9	0.998
	SC	0-6	35640	-2.1	2.6	3.3	0.989
	SC	0-3	28080	-1.2	1.2	1.7	0.997
	SC	3-6	7020	-4.7	2.3	5.4	0.961

C. Algorithm Testing From Independent Simulated Data

SC and SW algorithms were applied to simulated data obtained from the TIGR and STD databases over the 108 emissivity spectra. Bias (LST retrieved from the algorithm minus the reference LST), standard deviation, and RMSE values are provided in Table II, including also the linear correlation coefficient. RMSEs for the SW algorithm over the whole range of water vapor values are around 1 K, with almost no bias. As commented in [9], the SC algorithm with atmospheric functions estimated from the approach versus the w fails for moderate to high w values (e.g., $w > 3$ g $\cdot$ cm^{-2}). Therefore, RMSEs for

the SC algorithm over the whole range of w values increase to 3–4 K, except for the TIGR_{1711} database, with an RMSE of 2 K. This last result is explained by the w distribution, which is biased toward low values of w in this database. When only atmospheric profiles with w values lower than 3 $\text{g} \cdot \text{cm}^{-2}$ are selected, the SC algorithm provides RMSEs around 1.5 K, with almost equal values of bias and standard deviation, around 1 K in both cases (with a negative bias, thus the SC underestimates the LST). In contrast, when only w values higher than 3 $\text{g} \cdot \text{cm}^{-2}$ are considered, the SC algorithm provides RMSEs higher than 5 K. In these cases, it is preferable to calculate the atmospheric functions of the SC algorithm directly from (3) rather than approximating them by a polynomial fit approach as given by (4).

V. Discussion and Conclusion

The two Landsat-8 TIR bands allow the intercomparison of two LST retrieval methods based on different physical assumptions, such as the SC (only one TIR band required) and SW algorithms (two TIR bands required). Direct inversion of the radiative transfer equation, which can be considered also as an SC algorithm, is assumed to be a "ground-truth" reference under the condition that the information about the atmosphere ($\tau, L_u,$ and L_d) is accurate enough. The SC algorithm presented in this letter is a continuation of the previous SC algorithm developed for Landsat-4 and Landsat-5 TM sensors, as well as the ETM+ sensor on board the Landsat-7 platform [9], and it could be used to generate consistent LST products from the historical Landsat data using a single algorithm. An advantage of the SC algorithm is that, apart from surface emissivity, only water vapor content is required as input. However, it is expected that errors on LST become unacceptable for high water vapor contents (e.g., > 3 $\text{g} \cdot \text{cm}^{-2}$). This problem can be partly solved by computing the atmospheric functions directly from τ, L_u, and L_d values [see (5)], or also by including air temperature as input [15]. A main advantage of the SW algorithm is that it performs well over global conditions and, thus, a wide range of water vapor values; and that it only requires water vapor as input (apart from surface emissivity at the two TIR bands). However, the SW algorithm can be only applied to the new Landsat-8 TIRS data, since previous TM/ETM sensors only had one TIR band.

The LST algorithms presented in this letter were tested with simulated data sets obtained for a variety of global atmospheric conditions and surface emissivities. The results showed RMSE values of typically less than 1.5 K, although for the SC algorithm, this accuracy is only achieved for w values below 3 $\text{g} \cdot \text{cm}^{-2}$. Algorithm testing also showed that the SW errors are lower than the SC errors for increasing water vapor, and vice versa, as demonstrated in the simulation study presented in Sobrino and Jiménez-Muñoz [18]. Although an extensive validation exercise from *in situ* measurements is required to assess the performance of the two LST algorithms, the results obtained for the simulated data, the sensitivity analysis, as well as the previous findings for algorithms with the same mathematical structure give confidence in the algorithm accuracies estimated here.

References

[1] J. R. Irons, J. L. Dwyer, and J. A. Barsi, "The next Landsat satellite: The Landsat Data Continuity Mission," *Remote Sens. Environ.*, vol. 122, pp. 11–21, 2012.

[2] D. A. Quattrochi and J. C. Luvall, "Thermal infrared remote sensing data for analysis of landscape ecological processes: Methods and applications," *Landscape Ecolog*, vol. 14, no. 6, pp. 577–598, Dec. 1999.

[3] J. D. Kalma, T. R. McVicar, and M. F. McCabe, "Estimating land surface evaporation: A review of methods using remotely sensed surface temperature data," *Surveys Geophys.*, vol. 29, no. 4/5, pp. 421–469, Oct. 2008.

[4] W. Kustas and M. Anderson, "Advances in thermal infrared remote sensing for land surface modeling," *Agric. Forest Meteorol.*, vol. 149, no. 12, pp. 2071–2081, Dec. 2009.

[5] Z.-L. Li, B.-H. Tang, H. Wu, H. Ren, G. Yan, Z. Wan, I. F. Trigo, and J. A. Sobrino, "Satellite-derived land surface temperature: Current status and perspectives," *Remote Sens. Environ.*, vol. 131, pp. 14–37, Apr. 2013.

[6] Z.-L. Li, H. Wu, N. Wang, S. Qiu, J. A. Sobrino, Z. Wan, B.-H. Tang, and G. Yan, "Land surface emissivity retrieval from satellite data," *Int. J. Remote Sens.*, vol. 34, no. 9/10, pp. 3084–3127, 2013.

[7] A. M. Mika, "Three decades of Landsat instruments," *Photogramm. Eng. Remote Sens.*, vol. 63, no. 7, pp. 839–852, Jul. 1997.

[8] J. A. Barsi, J. R. Schott, F. D. Palluconi, D. L. Helder, S. J. Hook, B. L. Markham, G. Chander, and E. M. O'Donnell, "Landsat TM and ETM+ thermal band calibration," *Can. J. Remote Sens.*, vol. 29, no. 2, pp. 141–153, 2003.

[9] J. C. Jiménez-Muñoz, J. Cristóbal, J. A. Sobrino, G. Sòria, M. Ninyerola, and X. Pons, "Revision of the single-channel algorithm for land surface temperature retrieval from Landsat thermal-infrared data," *IEEE Trans. Geosci. Remote Sens.*, vol. 47, no. 1, pp. 339–349, Jan. 2009.

[10] L. M. McMillin, "Estimation of sea surface temperatures from two infrared window measurements with different absorption," *J. Geophys. Res.*, vol. 80, no. 36, pp. 5113–5117, 1975.

[11] J. A. Sobrino, Z.-L. Li, M. P. Stoll, and F. Becker, "Multi-channel and multi-angle algorithms for estimating sea and land surface temperature with ATSR data," *Int. J. Remote Sens.*, vol. 17, no. 11, pp. 2089–2114, 1996.

[12] J. C. Jiménez-Muñoz and J. A. Sobrino, "Split-window coefficients for land surface temperature retrieval from low-resolution thermal infrared sensors," *IEEE Geosci. Remote Sens. Lett.*, vol. 5, no. 4, pp. 806–809, Oct. 2008.

[13] A. Beck, G. P. Anderson, P. K. Acharya, J. H. Chetwynd, L. S. Bernstein, E. P. Shettle, M. W. Matthew, and S. M. Adler-Golden, *MODTRAN4 User's Manual*. Hanscom AFB, MA, USA: Air Force Res. Lab., 1999.

[14] A. M. Baldridge, S. J. Hook, C. I. Grove, and G. Rivera, "The ASTER spectral library version 2.0," *Remote Sens. Environ.*, vol. 113, no. 4, pp. 711–715, Apr. 2009.

[15] J. Cristóbal, J. C. Jiménez-Muñoz, J. A. Sobrino, M. Ninyerola, and X. Pons, "Improvements in land surface temperature retrieval from the Landsat series termal band using water vapor and air temperature," *J. Geophys. Res.*, vol. 114, no. D8, p. D08103, 2009.

[16] D. P. Dee, S. M. Uppala, A. J. Simmons, P. Berrisford, P. Poli, S. Kobayashi, U. Andrae, M. A. Balmaseda, G. Balsamo, P. Bauer, P. Bechtold, A. C. M. Beljaars, L. van de Berg, J. Bidlot, N. Bormann, C. Delsol, R. Dragani, M. Fuentes, A. J. Geer, L. Haimberger, S. B. Healy, H. Hersbach, E. V. Hólm, L. Isaksen, P. Kallberg, M. Kohler, M. Matricardi, A. P. McNally, B. M. Monge-Sanz, J.-J. Morcretter, B.-K. Park, C. Peubey, P. de Rosnay, C. Tavolato, J.-N. Thépaut, and F. Vitart, "The ERA-Interim reanalysis: Configuration and performance of the data assimilation system," *Q. J. R. Meteorol. Soc.*, vol. 137, no. 656, pp. 553–597, 2011.

[17] C. Mattar, C. Durán-Alarcón, J. C. Jiménez-Muñoz, and J. A. Sobrino, "Global Atmospheric Profiles from Reanalysis Information (GAPRI): A new dataset for forward simulations in the thermal infrared region," *IEEE Trans. Geosci. Remote Sens.*, 2014, submitted for publication.

[18] J. A. Sobrino and J. C. Jiménez-Muñoz, "Land surface temperature retrieval from thermal infrared data: An assessment in the context of the surface processes and ecosystem changes through response analysis (SPECTRA) mission," *J. Geophys. Res.*, vol. 110, no. D16, p. D16103, 2005.